ORIGINAL SCIENTIFIC PAPER

CROATICA CHEMICA ACTA

Croat. Chem. Acta **2021**, *94*(1)
Published online: August 2, 2021
DOI: 10.5562/cca3731

HKD 1926

An Estimate of a Frequency Characterizing the Electrochemical Stability of a Gold Electrode Modified by MHDA Thiol in Different Ways

Sarah Chaibi,[1] Mokhtar Zabat,[1,2,*] Toufik Hadjersi,[3] Seddik Elhak Abaidia,[1,2] Nadia Zine,[4] Nourdin Yaakoubi,[5] Abelhamid Errachid[4]

[1] Physics Department, M'hamed Bouguera University, Boumerdes, Algeria
[2] Laboratory of Coatings, Materials and Environment, UMBB, Boumerdes, Algeria
[3] Research Unit UDTS/CRTSE2, bd Frantz Fanon, Algiers, Algeria
[4] Institut des sciences Analytiques (ISA), Université Claude Bernard, Lyon1,UMR 5280, rue de la Doua,69100 Villeurbanne, Lyon 6, France
[5] M.C. Université du Maine –Rue Aristote – 72085 le Mans cedex 9 France
* Corresponding author's e-mail address: m_zabat@univ-boumerdes.dz

RECEIVED: January 14, 2021 * REVISED: June 9, 2021 * ACCEPTED: June 11, 2021

Abstract: A theoretical investigation aimed at estimating a characteristic frequency in the medium-low frequency domain in which the impedance response of a given interface measured by electrochemical impedance spectroscopy (EIS) is almost constant, constitutes the basic idea of this work. A theoretical model was subsequently applied to the data resulting from EIS measurements performed on gold electrodes modified by various ways of 16-mercaptohexadecanoic acid (MHDA) thiol functionalization. Analysis of these data revealed a direct relationship between the way the substrate was modified and this characteristic frequency.

Keywords: EIS, MHDA, functionalization, conductivity, dielectric frequency.

INTRODUCTION

ELECTROCHEMICAL biosensors are sensors based on affinity for certain entities. The detection principle is essentially based on the exploitation of the electrical data resulting from the variation of the signal on the modified electrode. Their design requires little energy resources involving relatively low cost, they also offer an ease to miniaturization. All this makes them very attractive as biosensors.[1,2,4–9] The most used electrochemical techniques to evaluate the variation of the surface deposit can be summarized as follows: differential voltametric pulse, cyclic voltammetry and chronoamperometry. The last ones are both transient techniques aimed at the analysis of electrochemical reactions. They provide the characteristics related to transport as well as thermodynamic phenomena.[10–18] EIS is one of the most powerful technique used to study interfaces,[18] based on the analysis of the impedance of the equivalent electrical circuit, it allows the quantification of the interfaces obtained by modification of the electrodes either spontaneously when they are immersed in electrolytes, or by electrodeposition, depending on the nature and the purpose of the work performed. Some of our recent works show the quantification of gold electrodes modified by different types of thiols.[19–21] Changes at the double layer of the electrode surface are detectable at low frequencies,[18,22] this requires large stabilization time of the harmonic cycles; hence the choice of the frequencies defining the experimental low frequencies range is crucial. The spontanious adsorption of self-assembled monolayer's (SAM's) of alkanethiolates on gold electrode has been the subject of numerous reports. Such SAMs-modified electrodes have been widely used in fundamental science and biosensing as ligand immobilization.[4,10,23–33] This is mainly due to the ability to form stable and suitable monolayers for different application domains simply by changing their end-groups. However, the performance of functional SAMs depends on many parameters such as concentration, incubation time, temperature, the nature of the solvent, and on the applied

potential in the case of an electrochemical characterization.[12] Various works based on frequency studies have been reported in the literature. Generally, the frequency lowest limit reached in the EIS measurements is in the order of 10 mHz.[34–40] The principal purpose of this work is to estimate a frequency limit defining a domain in the low frequency range, characterized by an impedance response tending to a steady state, with the aim to reduce the experiencing time. In this context experimental investigations were performed on different functionalization types of MHDA thiol by varying the incubation time and/or temperature, or by changing the electro-deposition potential for EIS measurements. The conductivity analysis of the thiol-modified gold electrode of MHDA, normalized with respect to the uncovered gold substrate ($\sigma_{Au\text{-}MHDA}$ / σ_{Au}), and of its real part ($\sigma_{Au\text{-}MHDA}$), has allowed to delimit the frequency domain in which the frequency variation has a small effect on the conductivity.

THEORETICAL APPROACH

The physical origin of the constant phase element (CPE) is a controversial subject to day. In practice, the CPE expresses a frequency dispersion of the electric double layer capacitance; its impedance is expressed as follows:

$$Z_{CPE} = \frac{1}{(j\omega)^n Q} \tag{1}$$

where j is the complex number, ω is the angular frequency ($\omega = 2\pi f$), Q is the frequency independent parameter and n is the CPE power. When $n = 1$, Q represents the pure capacitance, while for $n \neq 1$ the system shows behavior that has been attributed to the surface heterogeneity or to the continuously distributed time constants for charge transfer reactions.

For a parallel R-CPE combination (Figure 1.) the impedance becomes:

$$Z = \frac{R}{1 + (j\omega)^n RQ} \tag{2}$$

The measured impedance (Z) is the sum of a real part called resistance and an imaginary part named reactance,

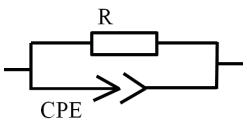

Figure 1. The R-CPE electrical circuit used in impedance modeling.

in the other terms:

$$Z = Z' - jZ'' \tag{3}$$

The real and the imaginary parts of Z are given by:

$$Z' = \frac{R\left[1 + \omega^n QR\cos(n\frac{\pi}{2})\right]}{(RQ)^2\omega^{2n} + 2\omega^n RQ\cos(n\frac{\pi}{2}) + 1} \tag{4}$$

$$Z'' = \frac{-R^2 Q\omega^n \sin(n\frac{\pi}{2})}{(RQ)^2\omega^{2n} + 2\omega^n RQ\cos(\frac{\pi}{2}n) + 1} \tag{5}$$

The phase displacement φ is given by:

$$\tan(-\varphi) = \frac{RQ\omega^n \sin(n\frac{\pi}{2})}{1 + RQ\omega^n \cos(n\frac{\pi}{2})} \tag{6}$$

On the other hand, the real part of the conductivity can be related to the impedance as follows:

$$real(\sigma) = \frac{d}{S}\left(\frac{Z'}{Z'^2 + Z''^2}\right) \tag{7}$$

where d is the thickness of the deposit and S is the active area of the electrode.

Its modulus is:

$$\sigma = \frac{d}{S}\left(\frac{Z'}{(Z'^2 + Z''^2)^{1/2}}\right) \tag{8}$$

Knowing that the conductivity of most disordered and ionic materials obeys to the Josher's universal power law:[18]

$$real(\sigma_{ac}) = \sigma_{dc} + A\omega^n \tag{9}$$

with

$$\sigma_{dc} = \frac{\varepsilon_0 \varepsilon_S}{\tau_\sigma} \tag{10}$$

σ_{dc} is the relaxation time conductivity, with:

$$\tau_\sigma = (RQ)^{1/n} \tag{11}$$

which is called the dielectric time.[18]

The frequency dispersion of the conductivity is then represented by $A\omega^n$ in many solid electrolytes; it expresses the CPE behavior when a periodic amplitude signal AC is applied.

The total conductivity in presence of dipolar relaxation processes has the following expression:

$$\sigma = \sigma_{dc} + A\omega^n + j\varepsilon_0\varepsilon\omega \quad (12)$$

Therefore the conductivity for a material with no dipolar relaxation (parallel RC circuit) is:

$$\sigma = \sigma_{dc} + j\varepsilon_0\varepsilon_s\omega \quad (13)$$

In the case of a non-dispersive conductivity its real part tends to ~ *(d / S.R)* at low frequencies, this expresses the invariability of the real (Z) with the frequency.

The presence of the *CPE* in the circuit introduces an ohmic loss $A\omega^n$ previously mentioned, which affects the conductivity in particular for the transport in disordered media far from a viscous media where the number of defects is insignificant.

The frequencies range in the laboratory measurements varies from 0.1Hz to 100 KHz. The model of the conduction in this domain is principally governed by the ionic conduction by hop of the charge carrier in the well system potential created by the particles in the medium, and by relaxations phenomena related to the polarization.[41] Two types of relaxations are considered; the relaxation by deformation and the interfacial relaxation.[42]

THEORETICAL RESULTS

According to the Josher's power law[18] the conductivity is said non dispersive when *Z'* tends to *R*. Referring to the model circuit made up by a resistance *R* connected in parallel to a capacitance C, the real part of the impedance is equals to 90 % *R* at $f = 0.3\ f_\tau$, where f_τ is the dielectric frequency defined at the maximum of the imaginary part of the impedance. It can be considered that from this frequency, the real part of the impedance is practically independent of the frequency.

In another hand at $f = 0.3\ f_\tau$ the [Eq. (4)] becomes:

$$Z' = \frac{R\left[1 + (0.3)^n \cos(n\frac{\pi}{2})\right]}{(0.3)^{2n} + 2\cdot(0.3)^n \cos(n\frac{\pi}{2}) + 1} \quad (14)$$

The plot of the real part of the impedance *Z'* against *n* for $0.66 < n < 1$ which is corresponding to $0.5 < \cos(n\pi/2) < 1$ is illustrated by the curve (Figure 2a). Knowing that $\cos(n\pi/2)$ represents the fraction of the dissipation energy Diss (%) of each harmonic cycle.[43] This curve shows that as soon as α approaches 0.85, we have *Z'* tends to *0.9R* with an accuracy of 6 %. Therefore, from this limit corresponding to $f = 0.3\ f_\tau$, it can be considered that the modulus of the impedance is not affected by the variation of the frequency, and that the CPE identifies with a capacitance.

When the value of the real part of the impedance *(Z')* is 0.9 *R*, the relation (4) gives:

$$f_{min} = \frac{f_\tau}{9^{1/n}}\left[-4\cos n\frac{\pi}{2} + \left[16(\cos n\frac{\pi}{2})^2 + 9\right]^{1/2}\right]^{1/n} \quad (15)$$

where f_{min} is a characteristic frequency defined the low boundary bandwidth in which the faradic current is considered as constant.

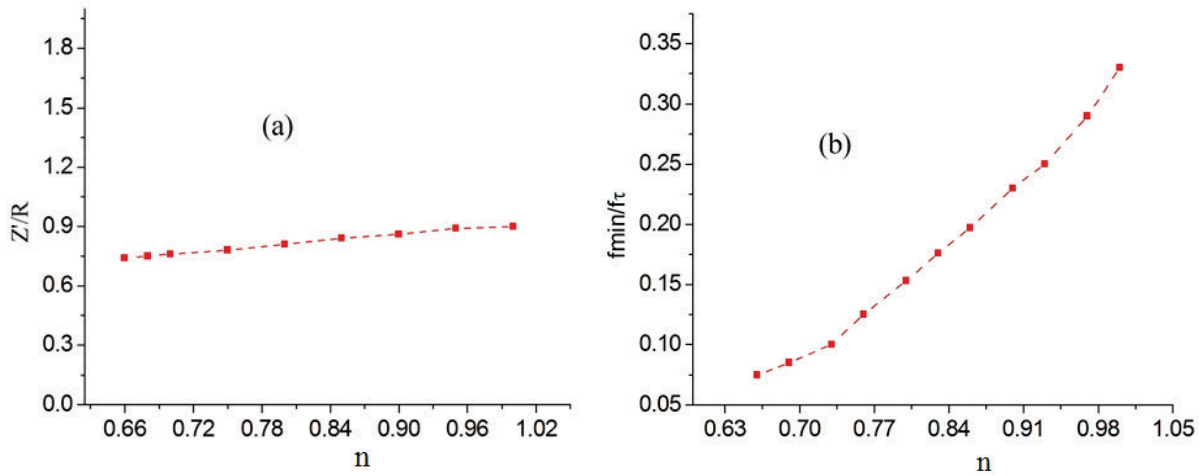

Figure 2. (a) Relative variation of real part of the impedance versus *n*. (b) relative variation of f_{min} versus *n* for $0.66 < n < 1$.

For simplicity we introduce a function:

$$g(n) = \frac{\left[-4\cos n\frac{\pi}{2} + \left[16(\cos n\frac{\pi}{2})^2 + 9\right]^{1/2}\right]^{1/n}}{9^{1/n}} \quad (16)$$

such that f_{min} can be written as:

$$f_{\min} = g(n) f_{\tau} \quad (17)$$

The nearby plot (Figure 2b) shows a curve varying linearly with n and tending to a limit of 0.3 f_{τ} (n = 1) corresponding to an RC parallel circuit.

On the other hand, for n greater than 0.95, thus $g(n)$ tends to:

$$g(n) \approx \frac{1}{3^{1/n}} \quad (18)$$

with an accuracy of 7 %, it leads to:

$$f_{\min} \approx \frac{f_{\tau}}{3^{1/n}} \quad (19)$$

Then:

$$f_{\min} \approx \frac{1}{2\pi(3RQ)^{1/n}} \quad (20)$$

According to the relation (20), the real part of the current tends to zero as soon as f is less than f_{min}, this corresponds in term of a dielectric time to a period T greater than $(3\ R\ Q)^{1/n}$. The dielectric time t -the invert of f_{min}- evolves according to the value of n in (20). For n comprised between 0.66 and 0.95 this time is approached by:

$$\tau \approx \left[\frac{(3RQ)^{\frac{1}{n}-1}}{3^{1/n} g(n)}\right] 3RQ \quad (21)$$

When n is close to unity (0.95 < n < 1), this time is estimated as:

$$\tau \approx \left[(3RQ)^{\frac{1}{n}-1}\right] 3RQ \quad (22)$$

At the limit value of n equal to the unity, this time is given by:

$$\tau = 3RQ \quad (23)$$

This show that the dielectric time for these particular values given by relations (21), (22) and (23) decreases when n evolves from 0.66 to 1 and that the *R-CPE* parallel circuit evolves towards an *R-C* parallel circuit, with a limit dielectric time value *(3 R Q)* for n equal to the unity. This is the ultimate case of an insulating defects-free substrate.

ELABORATION PROCEDURE OF MHDA SELF-ASSEMBLED MONO-LAYERS ON GOLD ELECTRODE

Materials used in elaboration procedure are 16-mercapto-hexadecanoic acid (MHDA), phosphate buffered saline (PBS), potassium ferrocyanide [$K_4[Fe(CN)_6]$] and potassium ferricyanide [$K_3[Fe(CN)_6]$] from Sigma-Aldrich. Gold macro-electrodes with an active surface of 0.503 cm^2 were cleaned with acetone, rinsed with ethanol and de-ionized water, then cleaned one time again 15 min with acetone at 60 °C in ultrasonic bath, and then dried with a stream of N_2. Subsequently the electrodes were irradiated with UV for 30 minutes, and then immerged in piranha solution for 3 minutes and immediately dipped into ethanol solution of 10 mM (MHDA).

Working electrodes were functionalized straightaway separately by one of the following ways:

a. Incubated overnight at θ = 4 °C
b. Incubated 1h15min at θ = 55 °C
c. Incubated 1h15min at θ = 55 °C followed by 1 h at θ = 4 °C
d. Electrodeposited by the chrono-amperometry at a potential of E = –0.5 V for 11 minutes in a solution containing 5 mM of MHDA diluted into 20 % of NaOH, 70 % of ethanol and 10 % of ionized water.

Finally, the electrodes were rinsed with ethanol and dried with N_2 flow.

EXPERIMENTAL, RESULTS AND DISCUSSION

Bio-Logic potentiostats equiped with EC-Lab software was used to measure the electrochemical spectroscopy of impedance (EIS) of SAMs at the interface solution/electrode at room temperature and in the presence of 5 mM of $K_4[Fe(CN)_6]$ / $K_3[Fe(CN)_6]$ redox probe in PBS solution at pH 7.4, using a modulation voltage 5 mV versus Ag/AgCl reference electrode. Some electrodes were submitted to various potentials so that once reproducible cycles were obtained one switches to another potential (Figures 3a and 3b). The EC-lab software modeling program was used to fit

impedance data. The dotted lines represented in the figures tend to a final frequency corresponding to the frequency in which the impedances Z equal to R_{ct} ($Z'' = 0$). They were evaluated by a suitable fitting from the imaginary part of the impedance curves versus the frequency.

The real and imaginary parts of the impedance as a function of the frequency, of SAMs-modified electrodes subjected to variable potentials are shown above (Figure. 3). The graph shows increasing curves as a function of the potential. They are evolving similarly to those obtained on a naked gold electrode subjected to an increasing polarization up to a potential value, close to the zero charge potential (PZC) of the electrode bare gold (0.18 V).[3]

The subsequent curve (Figure 4) depicts the variations of the real and the imaginary parts of the impedance versus

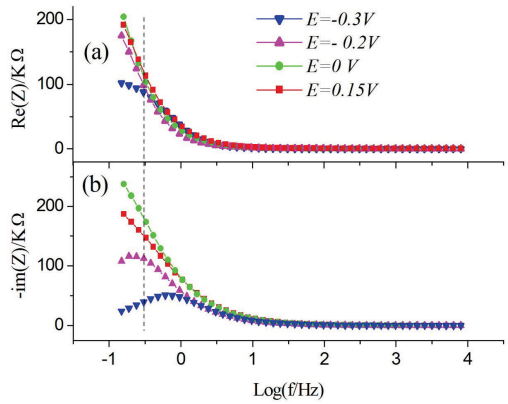

Figure 3. Variation of *Im(Z)* (b) and *Real (Z)* (a) of gold electrode functionalized by MHDA overnight at θ = 4 °C under different potentials.

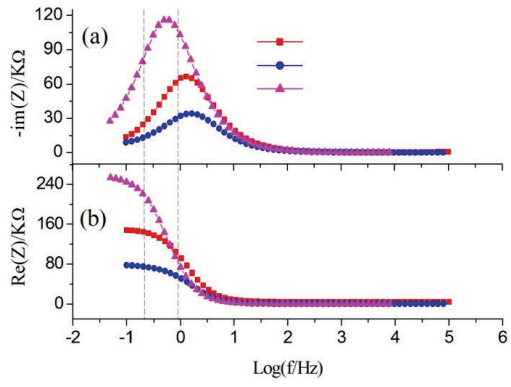

Figure 4. Variation of *-Im(Z)* (a) and *Real (Z)* (b) of *MHDA* modified gold electrode versus frequency for the applied potential E = –0.3 V. (▲) 1 h 15 min at θ = 55 °C then for 1 h at θ = 4 °C, (■) overnight at θ = 4 °C and (●) θ = 55 °C for 1 h 15 min.

frequencies of SAMs for different temperatures and incubation times. The highest value of the dielectric frequency corresponds to the *SAM*-modified electrode, functionalized at θ = 55 °C for 1 hour 15 min, while the smallest value corresponds to the functionalization by the succession of two incubations: one during 1 hour 15 minutes at θ = 55 °C, followed by another for 1 hour at θ = 4 °C. As the dielectric conductivity [Eq. (10)] and [Eq. (11)] predict, the two conductive and insulating (blocking) behaviors are to be considered for these two cases.

The normalized conductivity of SAMs-modified gold electrode plotted in Figure 5 (from the dielectric frequency) depicts decreasing curves exhibiting a tendency of SAMs toward an ordered and stable state.

This with the exception of the SAMs-modified electrode under E = –0.3 V polarization (Figure 5b), that shows decreasing curves in almost uniform way compared to that not subjected to any polarization (Figure 5a), where the normalized conductivity plot illustrates a curve almost flat, and evolving with a higher magnitude order. This result could indicate that SAMs are not stable, evolving slowly to an ordered state, and developing defects which favor the adsorption of the ferrocynate on the SAMs/gold interface.

This is why the relative conductivity is in the same magnitude order that of the bare gold electrode at equivalent conditions (important charge transfer through the pinholes).

Note that during conductivity measurements it is clear that it is difficult to go to frequencies that are too low of the order of mHz, because this requires a considerable time for the acquisition of a single value, therefore the

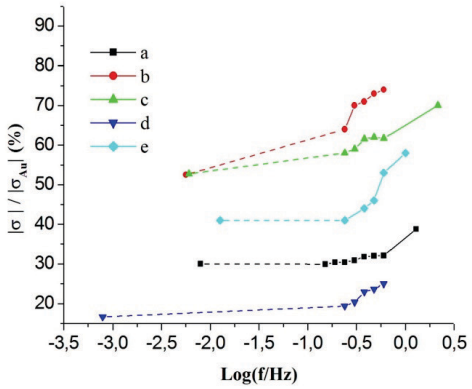

Figure 5. Normalized conductivity modulus versus frequency at applied potential –0.3 V for gold electrodes functionalized in different ways by MHDA thiol. a) overnight incubation at θ = 4 °C, b) overnight incubation at θ = 4 °C under –0.3 V polarization, c) 1 h 15 min incubation at θ = 55 °C, d) 1 h 15 min at θ = 55 °C and then 1 h at θ = 4 °C, e) electrodeposition for t = 11 min at E = –0.5 V.

noise can affect the measurements, so we extrapolated the graph obtained experimentally up to the calculated value deduced from the theoretical model. This allowed us to conclude that the normalized conductivity modulus remain almost constant, corresponding to Z modulus equal to the charge transfer resistance ($Z = R_{ct}$).

As illustrated by the curves of figure 6, the normalized real part of the conductivity varies as a function of the frequency with an order of magnitude between 1 and 1.3 and obeys the universal power law of Josher (12). The plots belonging to the dotted area vary in an order of magnitude between 1 and 1.1. It represents the region in which the real part of the conductivity is quite equal to that of $Z' = R_{ct}$, and the graphs of *MHDA*-thiol types where the conductivity is almost frequency-independent if one considers that the small variations (curves: a, d and e) result from the dipole relaxation in this region as predicted by Josher's universal power law (9) and (13), where $A\,\omega^{\alpha}$ can be neglected. Regarding the values of f_{min} extracted from Figure 6 recorded with their corresponding theoretical values f_{min} (α) and summarized in Table 1, we can notice that they are more and less the same as predicted by the model. The plot of Figure 7 graphically represents the variation of the normalized real part of the conductivity as a function of the phase shift. Plots inside the dotted zone have a lower ratio than 1.1, and the phase shift in this region is decreasing until zero, which corresponds to the state at $Z' = R_{ct}$ (thus Z'' is zero). The small variations in the conductivity ratio as a function of the phase shift shown by some of the plots (b, e and d) indicate that the plots deviate a little from Josher's universal power law (9), however, this remains insignificant, and the contribution of the capacitive current to the total current is small, with a general tendency towards a faradic current, which is in good agreement with the normalized conductivity plots shown in Figure 5.

In summary, as we have been interested in parameters such as a characteristic frequency at which the faradic current is considered constant, and a resistance R_{ct} which express the transfer of charges through the interface of the electrolyte with the electrode modified with gold. The Nyquist curves corresponding to the results obtained by EIS and modeled by a loop R-CPE are drawn up in Figure 8.

And since the charge transfer occurs at medium and

Table 1. Variation of the dielectric frequency measured at E = –0.3 V for various functionalization ways of MHDA, and the corresponding minimal frequencies: theoretical $f_{min}(\alpha)$ and f_{min} deduced from Figure 6.

Functionalization way of MHDA	n	$f_{min}(n)$ / Hz	f_{τ} / Hz	f_{min} / Hz
θ = 4 °C, t = 12 h, V = –0.3 V	0.97	0.17	0.6	0.24
θ = 4 °C, t = 12 h	0.96	0.36	1.25	0.30
θ = 55 °C, t = 1 h 15 min	0.93	0.43	1.7	0.58
θ = 55 °C, 1 h 15 min then θ = 4 °C, t = 1 h	0.95	0.17	0.6	0.24
Electrodeposited at V= –0.5 V for t = 11 min	0.94	0.27	1	0.24

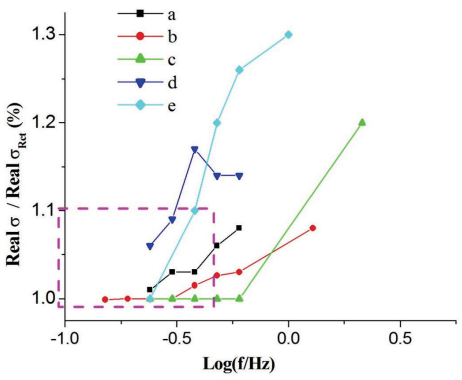

Figure 6. Normalized real part of the conductivity measured against frequency at applied potential –0.3 V for gold electrodes functionalized in different ways by *MHDA* thiol. a) overnight incubation at θ = 4 °C under –0.3 V polarization, b) overnight incubation at θ = 4 °C, c) 1 h 15 min incubation at θ = 55 °C, d) 1 h 15 min at θ = 55 °C and then 1h at θ = 4 °C, e) electrodeposition for t = 11 min at –0.5 V.

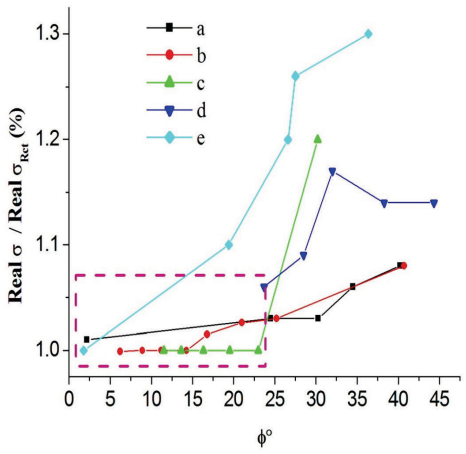

Figure 7. Normalized real part of the conductivity measured versus phase displacement at applied potential –0.3 V for gold electrodes functionalized in different ways by MHDA thiol. a) overnight incubation at θ = 4 °C under –0.3 V polarization, b) overnight incubation at θ = 4 °C, c) 1 h 15 min incubation at θ = 55 °C, d) 1 h 15 min at θ = 55 °C and then 1 h *at* θ = 4 °C, e) electrodeposition for t = 11 min at –0.5 V.

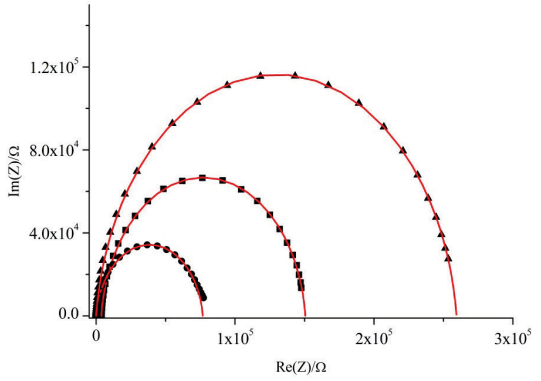

Figure 8. Nyquist diagram of MHDA modified gold electrode versus frequency for the applied potential E= –0.3 V. (▲) 1 h 15 min at θ = 55 °C then for 1h at θ = 4 °C, (■) overnight at θ = 4 °C and (●) θ = 55 °C for 1 h 15 min. Solid lines correspond to ideal semicircles.

Table 2. Values of EEC elements extracted from EIS measurements for different elaboration modes. With R_{el} = 24 Ω.

Functionalization way of MHDA	R_{ct} / Ω	$Q[F.s^{(n-1)}]$	n
θ = 4 °C, t = 12 h, E= –0.3 V	109560	2.35×10^{-6}	0.95
θ = 4°C, t = 12 h	146750	0.95×10^{-6}	0.95
θ = 55 °C, t = 1 h 15 min	76296	1.57×10^{-6}	0.93
θ = 55 °C, 1 h 15 min then θ = 4 °C, t = 1 h	25942	1.18×10^{-6}	0.93
Electrodeposition at E= –0.5 V , t = 11 min	103640	2.38×10^{-6}	0.84

high frequencies, we opted for an equivalent circuit consisting of an R_{ct}-CPE loop in series with the electrolyte resistance R_{el} which is almost constant and very weak comparing to R_{ct}. It turns out that this circuit describes our interface faithfully. For certain modes of elaboration (θ = 4 °C, θ = 55°C + θ = 4°C, E = –0.3 V), all the points obtained experimentally can be included in this EEC, however for others (θ = 55°C, Electrodeposition). The deviations of the experimental values from the ideal semicircles are visible between the symbols and solid lines. The last two points of the Nyquist representation go slightly out of the fit curve obtained with Zsim software. As these points are generally attributed to the phenomena of diffusions through the SAMs, caused by the local imperfections of the SAMs and / or due the roughness of the substrate itself,[21] and which are not the aim of this work, we have excluded them from the equivalent circuit so as not to bias the values of R_{ct} and CPE elements. The results of the fitting of the data obtained by EIS are drawn up in the Table 2. Fit errors are not exceeding 3 %. R_{el} values can be deduced directly from the

Table 3. Symbols used in this manuscript gathered as well as their meanings.

Symbol	Meaning
Q(CPE)	The frequency independent parameter or the coefficient of CPE
Z_{CPE}	Impedance of the constant phase element.
n	Exponent in the CPE: 0 < n <1
ω	Pulsation
J	Imaginary number j=√-1
R	Resistance
R_{ct}	Resistance to charge transfer
Z	Impedance
Z'	Real part Impedance Z
Z''	Imaginary part of Impedance Z
σ	Ionic conductivity
σ_{dc}	Frequency independent ionic conductivity
σ_{ac}	Frequency dependent conductivity
A	Temperature dependent factor
ε_0	Vacuum dielectric constant
ε_s	Static dielectric constant
τ_σ	Relaxation time
S	Active area of the electrode
d	Thickness of the deposit
f_{min}	A frequency characteristic of the invariability of the faradic current

offset of the Nyquist semicircle from the Z_{im} axis. The salient point in these results is that the value of the exponent n is very close to 1, which is the value for a perfect capacitor. It is around 0.93 for the different elaboration methods, except for the case of electrodeposition where it is 0.84. The high values of R_{ct} and low of Q respectively reflect the quality of the resulting coating relative to the bare gold electrode.

CONCLUSION

The main problem with electrochemical sensors is to delineate the low frequency threshold where key parameters such as charge transfer resistance R_{ct}, used to quantify any changes occur on the surface. Based on the analogy between the impedances of a loop in R-CPE and another in RC, we tried to delimit the low frequency threshold obtained with a circuit in R-CPE, beyond the electric current is almost stable. This analogy made it possible to correlate the low frequency limit with the dielectric frequency (f_τ) of the ligand through a multiplicative factor $g(n)$. This result is confirmed when applied to the analysis of the real part of the conductivity and / or to the normalized total conductivity

of gold electrodes modified by three types of thiol SAMs. We also note that from the characteristic frequency of the ligand [$g(n)$ f_τ], the real part of the current function does not evolve too much. This is particularly interesting for detection applications when the sensor is exposed to different ligand concentrations and for which the formation time of each deposited layer is closely related to the low frequency domain. When this time is evaluated from [$g(n)$ f_τ] of the receiver, it should facilitate the exploitation of the data by the optimization of the response time of the experiments, particularly when f_τ is of the order of some Hertz; knowing that in terms of time, an harmonic cycle of EIS is meanly spent in the last 10 mHz. This concept once applied, would allow considerable time savings in bio-detection, and consequently early diagnosis.

REFERENCES

[1] Y. Sun, Q. Ren, B. Liu, Y. Qin, S. Zhao, *Biosensors Bioelectronics* **2016**, *78*, 7–13. https://doi.org/10.1016/j.bios.2015.11.014

[2] C. Fernández-Sánchez, C.J. McNeil, K. Rawson, *Trends in Anal. Chem.* **2005**, *24*, 37–48. https://doi.org/10.1016/j.trac.2004.08.010

[3] S. Trasatti, *J. Electroanal. Chem. Interfacial Electrochem.*, **1971**, *33*, 351–378. https://doi.org/10.1016/S0022-0728(71)80123-7

[4] S. Vogt, Q. Su, C. Gutiérrez-Sánchez, G. Nöll, *Anal. Chem.* **2016**, *88*, 4383–4390. https://doi.org/10.1021/acs.analchem.5b04814

[5] L. El-Harrad, I. Bourais, H. Mohammadi, A. Amine, *Sensors* **2018**, *18*, 164. https://doi.org/10.3390/s18010164

[6] H. A. Abdulbari, E.A. Basheer, *ChemBioEng Rev.* **2017**, *4*, 92–105. https://doi.org/10.1002/cben.201600009

[7] J. M. Moon, N. Thapliyal, K.K. Hussain, R.N. Goyal, Y.B. Shim, *Biosensors Bioelectronics*, **2018**, *102*, 540–552. https://doi.org/10.1016/j.bios.2017.11.069

[8] D. Bizzotto, I.J. Burgess, T. Doneux, T. Sagara, H. Z. Yu, ACS sensors, 2018, 3, 5–12. https://doi.org/10.1021/acssensors.7b00840

[9] T. Balkenhohl, F. Lisdat, *Analyst* **2007**, *132*, 314–322. http://dx.doi.org/10.1039/b609832k

[10] Z. Nováková, R. Orinakova, A. Orinak, P. Hvizdos, A.S. Fedorková, *Electrochem. Sci.* **2014**, *9*, 3846–3863. https://doi.org/10.1016/j.bios.2014.01.038

[11] K. Uosaki, *Chem. Record* **2009**, *9*, 199–209. https://doi.org/10.1002/tcr.200900002

[12] M. Zabat, M. Morin, *Research Trans Tech Publications* **2013**, *626*, 514–517. https://doi.org/10.4028/www.scientific.net/AMR.626.514

[13] N. Muskal, D. Mandler, *J. Jerusalem. Current Separations* **2000**, *19*, 49–54.

[14] A. Molina, J. González, *Pulse voltammetry in physical electrochemistry and electroanalysis*, Springer, **2016**, 1–66.

[15] N. Ajami, A. Ehsani, F. Babaei, R. Safari, *J. Molecular Liquids* **2016**, *215*, 24–30. https://doi.org/10.1016/j.molliq.2015.12.023

[16] H. Gomez, G. Riveros, D. Ramirez, *Int. J. Electrochem. Sci.*, **2017**, *12*, 985–993. https://doi.org/10.20964/2017.02.09

[17] R. Schweiss, D. Pleul, F. Simon, A. Janke, P.B. Welzel, B. Voit, W. Knoll, C. Werner, *The Journal of Physical Chemistry B*, **2004**, *108*, 2910–2917. https://doi.org/10.1021/jp035724m

[18] E. Barsoukov, J. R. Macdonald, *Impedance spectroscopy: Theory, experiment, and applications*, John Wiley & Sons, **2018**, 1–21

[19] S. Hadjimi, A. Belayadi, M. Zabat, A. Mougari, M. W. Khemici, *J. Elec. Materi.* **2019**, *48*, 3908–3918. https://doi.org/10.1007/s11664-019-07151-4

[20] A. Belayadi, A. Mougari, M. Zabat, *J Solid State Electrochem.* **2019**, *23*, 195–204. https://doi.org/10.1007/s10008-018-4112-y

[21] A. Mougari, M. Zabat, S. Boudjadar, *Surface Review Letters* **2019**, *26*, 1950067. https://doi.org/10.1142/S0218625X19500677

[22] M. Raina, *Development of an impedimetric biosensor using a non-antibody based biological recognition molecule*, University of Leeds, UK, **2013**, 143. http://etheses.whiterose.ac.uk/id/eprint/6844

[23] X. Yu, Z. Wang, Y. Jiang, F. Shi, X. Zhang, *Advanced Materials* **2005**, *17*, 1289–1293. https://doi.org/10.1002/adma.200401646

[24] J. Lahann, S. Mitragotri, T.N. Tran, H. Kaido, J. Sundaram, I.S. Choi, S. Hoffer, G.A. Somorjai, R. Langer, *Science*, **2003**, *299*, 371–374. https://doi.org/10.1126/science.1078933

[25] S. E. Creager, J. Clarke, *Langmuir* **1994**, *10*, 3675–3683. https://doi.org/10.1021/la00022a048

[26] J. Lahann, R. Langer, *MRS bulletin*, **2005**, *30*, 185–188. https://doi.org/10.1557/mrs2005.50

[27] C. S. Weisbecker, M. V. Merritt, G. M. Whitesides, *Langmuir* **1996**, *12*, 3763–3772. https://doi.org/10.1021/la950776r

[28] E. Boubour, R. B. Lennox, *Langmuir* **2000**, *16*, 7464–7470. https://doi.org/10.1021/la000514b

[29] L. Cao, Q. Li, J. Ji, P. Yan, T. Wang, *J. Electrochem. Sci.* **2013**, *8*, 3074–3083. https://doi.org/10.1016/j.electacta.2013.01.029

[30] G. G. Matlou, D. Nkosi, K. Pillay, O. Arotiba, *Sensing Bio-Sensing Res.* **2016**, *10*, 27–33. https://doi.org/10.1016/j.sbsr.2016.08.003

[31] J. M. Devi, *Progress in Natural Science: Materials International*, **2014**, *24*, 405–411. https://doi.org/10.1016/j.pnsc.2014.06.009
[32] J. C. Love, L. A. Estroff, J. K. Kriebel, R. G. Nuzzo, G. M. Whitesides, *Chem. Rev.* **2005**, *105*, 1103–1170. https://doi.org/10.1021/cr0300789
[33] M. Smiljanić, C. Adam, T. Doneux, *J. Electroanal. Chem.* **2018**, *815*, 238–245. https://doi.org/10.1016/j.jelechem.2018.03.010
[34] A. Xu, F. Zhang, F. Jin, R. Zhang, B. Luo, T. Zhang, *Int. J. Electrochem. Sci.* **2014**, *9*, 5116–5125.
[35] G. R. Olhoeft, *Geophysics* **1985**, *50*, 2492–2503. https://doi.org/10.1190/1.1441880
[36] Z. Stević, M. R. Vujasinović, M. Radunović, *Sensors* **2009**, *9*, 7365–7373. https://doi.org/10.3390/s90907365
[37] C. L. Alexander, B. Tribollet, M. E. Orazem, *Electrochim. Acta*, **2015**, *173*, 416–424. https://doi.org/10.1016/j.electacta.2015.05.010
[38] M. Zhu, N. Zhang, H. Wang, Y.D. Li, S.G. Huang, Q.J. Li, Y. Yu, Y.M. Guo, X.L. Liu, C.C. Wang, *RSC Advances* **2017**, *7*, 26130–26135. https://doi.org/10.1039/C7RA00058H
[39] E. Karden, S. Buller, R. W. De Doncker, *Electrochim. Acta*, **2002**, *47*, 2347–2356. https://doi.org/10.1016/S0013-4686(02)00091-9
[40] B. Hirschorn, M. E. Orazem, B. Tribollet, V. Vivier, I. Frateur, M. Musiani, *J. Electrochem. Soc.* **2010**, *157*, 452–457. https://doi.org/10.1149/1.3499564
[41] M. Alonso, E. J. Finn, *Fundamental university physics: Fields and waves. Reading*, Addison-Wesley, **1980**, p. 110
[42] C. Kittel, P. McEuen, P. McEuen, *Introduction to solid state physics*, New York: Wiley, **2005**, p.455
[43] J. Tymoczko, W. Schuhmann, A. S. Bandarenka, *Electrochem. Comm.* **2013**, *27*, 42–45. https://doi.org/10.1016/j.elecom.2012.11.001